Supporting Information

Developing Two High-Nuclearity Ag Nanoclusters with Temperature-Sensitive Fluorescence Properties

Xiao-Lin Ye † [a], Sobhan Rezayati †[b], Fahime Bigdeli†[b], Le Yang [a], Kuan-Guan Liu [a], *, Jianyu Wei [a], *, Ali Morsali [b], *

[a] School of Materials and New Energy, Ningxia University, Yinchuan, Ningxia 750021, China

[b] Department of Chemistry, Faculty of Sciences, Tarbiat Modares University, P.O. Box 14115-175, Tehran, Iran.

*Corresponding Author: liukuanguan@nxu.edu.cn (K.-G. Liu); Jianyu.wei@nxu.edu.cn (J. Wei); morsali_a@modares.ac.ir (A. Morsali)

†These authors contributed equally to this work.

1. Experimental

1.1. Materials and Measurements

$(AgC{\equiv}CPh)_n$ was prepared according to the literature methods.[1] $(AgC{\equiv}CPh)_n$ are potentially explosive and should be used in small quantity and with much carefully. 0.1 M Me_4NOH solution was prepared by adding 0.3625 g (2 mmol) Me_4NOH to 20 mL CH_3OH. 0.1 mol/L $(NH_4)_2Mo_2O_7$ solution was prepared by adding 0.392 g (2 mmol) $(NH_4)_2Mo_2O_7$ and 1.631 g (9 mmol) Me_4NOH into 20 mL CH_3OH under the ultrasonic condition. All other reagents and solvents were commercially available from Aladdin and used as received without further purification. In the synthetic process, the 20 mL glass sealed bottles were used as reaction vessel. The FT-IR spectra were recorded from KBr pellets in the range 4000-400 cm^{-1} with a WQF-520A FT-IR spectrometer. The powder X-ray diffraction (PXRD) pattern was recorded with Advanced D8. The TGA curve was recorded on DSC-TGA SDT 650 (The samples were heated from 30 °C to 800 °C at 10 °C /min under a nitrogen atmosphere. The solid UV-vis diffuse reflectance spectra were recorded on a UV-2600 spectrophotometer at room temperature. Accurate Eg estimation in both clusters studied were obtained by using the general equation $(h\nu) \approx B\ (h\nu\text{-}Eg)^n$ (where a °F(R)) and indirect allowed transition.[2] Luminescence was measured using an Edinburgh FLS-1000 spectrometer. Quantum yield is determined

using the Quantaurus-QY's integrating sphere accessory in absolute quantum yield measurement mode. ESI-MS were performed on an Agilent Technologies ESI-TOF-MS. Qualitative analysis were carried out using GCMS-QP2010 Plus with EI ion source, EI-MS standard database, and an RTX-5 quartz capillary column. X-ray photoelectron spectroscopy (XPS) studies were performed on PHI Quantum-2000 XPS. The sample was put under UHV to reach the 10^{-8} Pa range. The non-monochromatized Al Kα source was used at 10 kV and 10 mA. All binding energies were calibrated using the C (1s) carbon peak (284.6 eV), which was applied as an internal standard. The organic elemental analyzer (EA) tests were performed using a German Elementar UNICUBE instrument, with the samples analyzed in both CHNS mode and O mode.

1.2. Crystal-Structure Determination and Refinement

X-ray-quality crystals of both clusters were grown from methanol at 5 °C, and X-ray crystallographic data were recorded by mounting single-crystals of (0.20 × 0.10 × 0.10 mm^3 for YL-1 and 0.22 × 0.13 × 0.09 mm^3 for YL-5) onto a glass fiber. Intensity data of both clusters were collected on a Bruker SMART APEX CCD diffractometer (Mo Kα source). Absorption corrections were applied by using the program CrysAlis (multi-scan). The structures were solved by SHELXT methods, and all non-hydrogen atoms were refined anisotropically by least-squares on F^2 using the SHELXTL program. The hydrogen atoms of organic ligands were generated geometrically. The difference map for this structure shows negative holes over 3 of the Ag atoms and their occupancies refine to 92-94% when freely refined. Nearby are the 3 largest residuals of around 2.5-3.5. These issues are therefore attributed to slight disorder in this region that could not be sensibly modelled.[3,4] The YL-1 crystal contains large solvent-accessible voids, and the contribution of solvent electron density was removed using the SQUEEZE routine. The TGA data shows that YL-1 begins to lose weight at 80°C, with the first weight loss percentage being approximately 1.1%, which is consistent with the theoretical weight loss corresponding to the inclusion of about one methanol molecule and one water molecule in the structure. The tetrafluoroborate anions in YL-1, as well as the methanol

molecules and trifluoromethanesulfonate anions in YL-5, were subjected to disordered refinement. Pertinent crystallographic data were presented in Table S**2** and selected bond lengths (Å) for a cluster were shown in Table S**3.**

1.3. Computational Details

Density functional theory (DFT) calculations were performed by using Gaussian 16 program.[5] For the sake of the computational limit, all the phenyl groups on the alkynyl and phosphate ligands were simplified by methyl groups. The generalized gradient approximation (GGA) corrections for exchange and correlation of Becke and Perdew (BP86 functional),[6,7] together with an all-electron Def2-SVP[8] basis set were used for geometry optimizations. Grimme's empirical DFT-D3 corrections were employed to take into account the London dispersion effects.[9] The optimized geometries were characterized as true minima on their potential energy surface by harmonic vibrational analysis.[10] These optimized structures were recalculated as single points under PBE0[11]/Def2-SVP level of theory. Excitation energies of the first 150 excited states were calculated by using time-dependent DFT (TD-DFT)[12] approach under PBE0/Def2-SVP level of theory. The molecular orbitals were generated by using an isovalue of 0.02 (e/bohr3) by using Multiwfn program.[13]

Table S1. Elemental Analysis of Clusters YL-1 and YL-5.

	N (%)	**C (%)**	**H (%)**	**S (%)**	**O (%)**
YL-1	0.00	38.00 (±0.05)	2.58 (±0.01)	0.00	7.18 (±0.04)
YL-5	0.00	39.09 (±0.01)	2.35 (±0.02)	0.63 (±0.01)	7.34 (±0.04)

Table S2. Table of crystallographic data for clusters YL-1 and YL-5.

Clusters	YL-1	YL-5
molecular formula	$(CrO_4)@Ag_{19}(PhC{\equiv}C)_7(Ph_2PO_2)_8(H_2O)\cdot(BF_4)_2\cdot(CH_3OH)$	$(MoO_4)@Ag_{19}(PhC{\equiv}C)_9(Ph_2PO_2)_7\cdot OTf\cdot 2CH_3OH$
Chemical formula	$C_{158}H_{143}Ag_{19}B_2CrF_8O_{28}P_8$	$C_{317}H_{242}Ag_{38}F_6Mo_2O_{45}P_{14}S_2$
Formula weight	5012.63	9673.73
Crystal system	Triclinic,	Monoclinic,
Space group	P-1	$P2_1$
a, Å	17.2664(6)	16.444(3)
b, Å	17.8141(6)	19.237(4)
c, Å	29.2674(9)	25.411(5)
α, deg	80.312(1)	90
β, deg	74.594(1)	107.47(3)
γ, deg	87.937(1)	90
V, Å^3	8554.6(5)	7668(3)
Z	2	1
ρ_{calc}, g/cm^3	1.946	2.095
μ, mm^{-1}	2.327	2.599
Reflections collected	193150	144557
Independent reflections	40337	36566
R_{int}	*0.0939*	*0.0429*
Data/restraints/parameters	*40337/3799/2065*	*36566/663/2016*
Final R indices [$I > 2\sigma(I)$[a,b]]	*0.059*	*0.0283*
R indices (all data)	*0.085*	*0.0344*
GOF on F^2	*1.076*	*1.069*
$\Delta\rho_{max}$, e Å^{-3}	*3.452*	*0.7*
$\Delta\rho_{min}$, e Å^{-3}	*-1.947*	*-0.64*

[a] $R_1 = [\Sigma\ abs(abs(Fo) - abs(Fc))]/ [\Sigma\ abs(Fo)]$. [b] $wR_2 = [\Sigma(w(Fo^2 - Fc^2)^2)/ \Sigma[w(Fo^2)^2]^{0.5}$

Table S3. Selected Bond Lengths (Å) for clusters YL-1 and YL-5.

Parameters	Bond Lengths (Å)	
	YL-1	YL-5
Ag-Ag	2.775(8)-3.366(8)	2.8047(10)-3.3722(9)
Ag-O	2.196(8)-2.592(6)	2.224(4)-2.585(4)
P-O	1.502(5)-1.528(5)	1.504(5)-1.529(5)
Cr-O (CrO_4^{2-})/Mo-O (MoO_4^{2-})	1.629(5)-1.680(5)	1.763(4)-1.792(4)

Table S4. Comparison of luminescence properties for structurally similar clusters to cluster YL-5.

Nanocluster	molecular formula	Temperature (K)	λ_{EM} (nm)	τ_{ave}	PLQY (%)	Reference
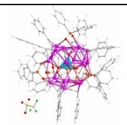	**$(MoO_4)@Ag_{19}(C{\equiv}CPh)_9(Ph_2PO_2)_7{\cdot}(OTf){\cdot}CH_3OH$**	77	497	450.85 μs	14.2	This work
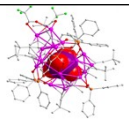	**$[(MoO_4)@Ag_{20}(C{\equiv}C^tBu)_8(Ph_2PO_2)_7(tfa)_2]\cdot(tfa)$**	77	507	47.87 μs	3.8	[14]
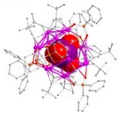	**$(MoO_4)@Ag_{18}(C{\equiv}C^tBu)_8(Ph_2PO_2)_7\cdot(OH)$**	77	516	4.85 μs	1.1	[14]
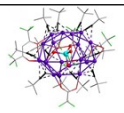	**$[MoO_4@Ag_{19}(^tBuC{\equiv}C)_{12}(hfac)_2(CF_3COO)_3]$**	-	-	-	-	[15]
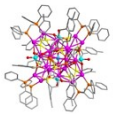	**$[MoO_4@Ag_{24}(MeC_6H_4S)_{12}(dppm)_6(MoO_4)_4]{\cdot}2BF_4{\cdot}C_2H_5NO$**	-	-	-	-	[16]
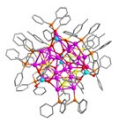	**$[MoO_4@Ag_{24}(MeC_6H_4S)_{12}(dppm)_6(MoO_4)_4]{\cdot}2CF_3SO_3$**	-	-	-	-	[16]
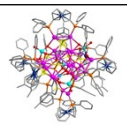	**$[MoO_4@Ag_{24}(MeC_6H_4S)_{12}(dppf)_6(MoO_4)_4]{\cdot}2CF_3SO_3$**	-	-	-	-	[16]
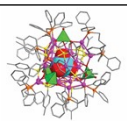	**$[MoO_4@Ag_{24}(MeC_6H_4S)_{12}(dppb)_6(MoO_4)_4]{\cdot}2CF_3SO_3$**	-	-	-	-	[16]
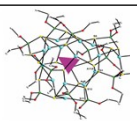	**$[Ag_{16}(MoO_4)\{S_2P(OEt)_2\}_{12}]_2(PF_6)_4$**	77	605	-	-	[17]

Table S5. Optimized metal-metal bond lengths in structural and single-crystal configurations

Bond	YL-1		Bond	YL--5	
	Experimental	DFT optimized		Experimental	DFT optimized
Ag01-Ag02	2.8545(8)	2.879	Ag1-Ag3	2.981(1)	2.940
Ag01-Ag0E	2.8928(8)	2.747	Ag1-Ag4	3.154(1)	3.232
Ag02-Ag0I	2.8660(8)	2.810	Ag1-Ag15	3.047(1)	2.949
Ag02-Ag05	3.3661(8)	3.442	Ag2-Ag4	2.806(1)	2.781
Ag03-Ag04	2.8855(8)	2.888	Ag2-Ag9	3.019(1)	2.930
Ag03-Ag08	2.9773(8)	2.990	Ag2-Ag12	2.847(1)	2.884
Ag03-Ag07	3.0068(8)	2.863	Ag2-Ag15	3.150(1)	2.968
Ag03-Ag0A	3.1564(8)	2.956	Ag3-Ag5	2.866(1)	2.855
Ag04-Ag07	3.0237(8)	2.867	Ag3-Ag15	2.874(1)	2.938
Ag04-Ag0A	3.1279(8)	3.163	Ag3-Ag17	3.111(1)	3.182
Ag05-Ag06	2.8148(8)	2.855	Ag4-Ag15	3.107(1)	2.982
Ag05-Ag08	3.0020(8)	2.856	Ag5-Ag13	3.065(1)	3.163
Ag06-Ag08	2.9932(8)	2.979	Ag5-Ag17	3.055(1)	3.067
Ag07-Ag0D	2.9183(8)	2.812	Ag6-Ag7	2.867(1)	3.102
Ag07-Ag0B	2.9324(8)	2.833	Ag6-Ag10	3.372(1)	2.997
Ag08-Ag0A	3.1433(8)	2.898	Ag6-Ag14	3.135(1)	2.928
Ag09-Ag0F	2.8234(8)	2.772	Ag6-Ag16	3.067(1)	2.900
Ag09-Ag0J	2.8732(9)	2.743	Ag6-Ag19	3.097(1)	2.929
Ag09-Ag0C	2.9617(8)	2.828	Ag7-Ag14	3.028(1)	2.920
Ag09-Ag0E	3.1344(8)	3.087	Ag7-Ag19	2.999(1)	2.830
Ag0B-Ag0D	3.0294(8)	2.933	Ag8-Ag9	2.822(1)	2.874
Ag0C-Ag0G	2.7746(8)	2.880	Ag8-Ag13	2.939(1)	2.816
Ag0C-Ag0F	2.8797(8)	2.823	Ag8-Ag17	2.948(1)	2.906
Ag0E-Ag0I	2.9729(8)	2.768	Ag8-Ag18	2.992(1)	2.834
Ag0F-Ag0G	3.1086(8)	2.945	Ag9-Ag12	3.068(1)	2.957
Ag0G-Ag0H	2.9776(8)	2.775	Ag9-Ag18	3.147(1)	2.851
Ag0H-Ag0I	3.0823(9)	3.001	Ag10-Ag12	3.663(1)	3.812
			Ag10-Ag14	2.804(1)	2.802
			Ag10-Ag16	2.914(1)	2.963
			Ag11-Ag16	3.002(1)	2.781
			Ag11-Ag19	2.914(1)	2.907
			Ag12-Ag18	3.243(1)	3.147
			Ag13-Ag17	3.152(1)	2.972

2. Characterization

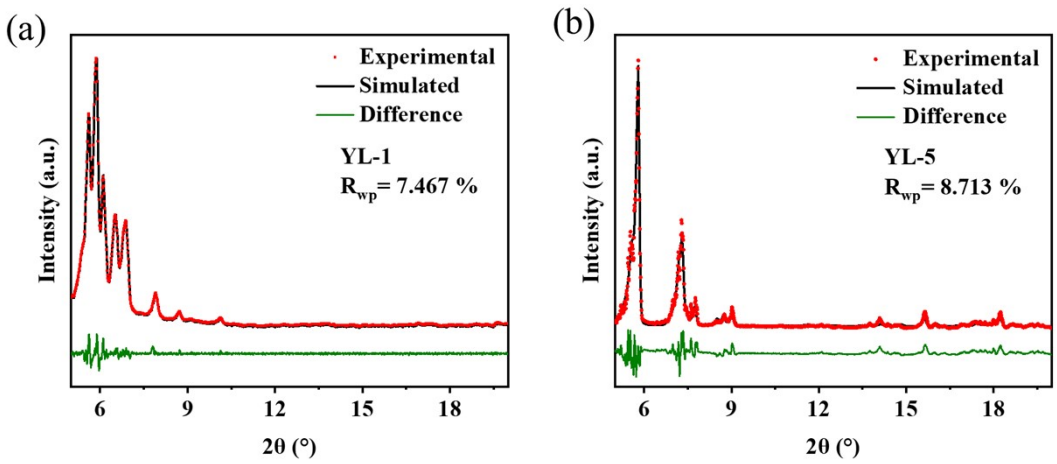

Figure S1. The powder XRD patterns of both clusters YL-1 and 2 YL-5 after Rietveld refinement analysis.

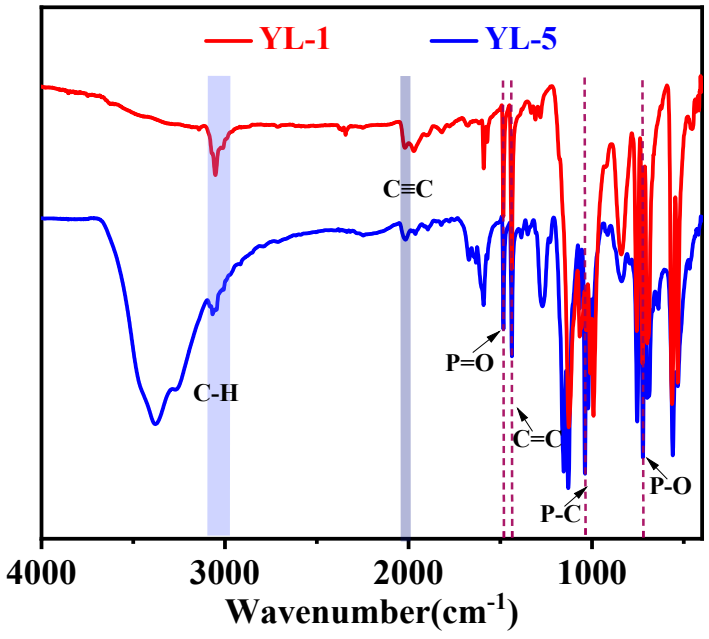

Figure S2. The IR spectra of both clusters 1 (YL-1) and 2 (YL-5).

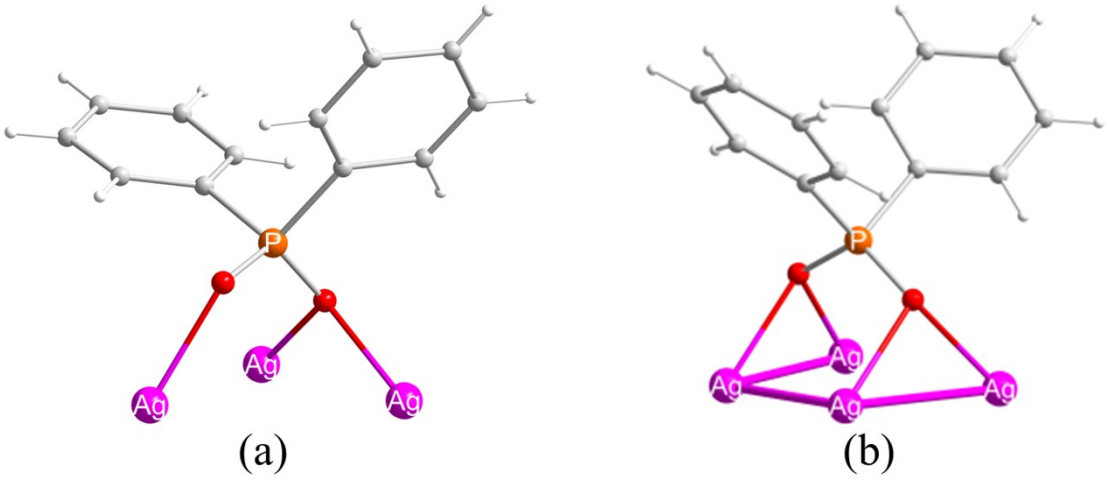

Figure S3. The μ_3:O_1,O_2 (a) and μ_4:O_2,O_2 (b) coordination modes of diphenylphosphonic acid ligands in cluster YL1.

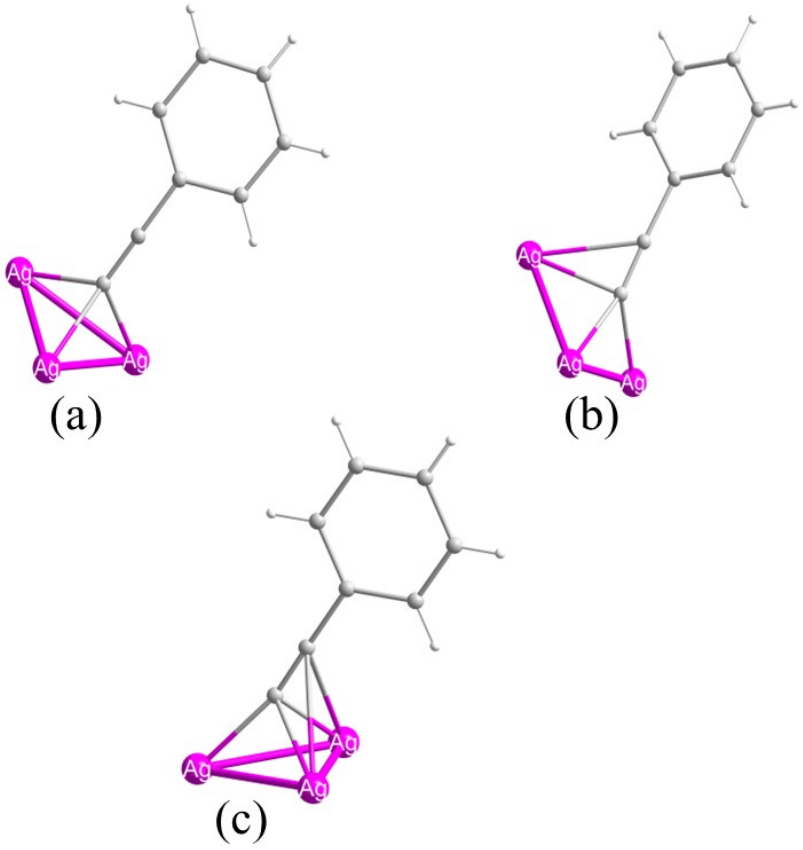

Figure S4. The μ_3-η^1,η^1,η^1 (a), μ_3-η^1,η^1,η^2 (b) and μ_3-η^1,η^2,η^2 (c) coordination modes of phenylethynyl ligands in cluster YL1

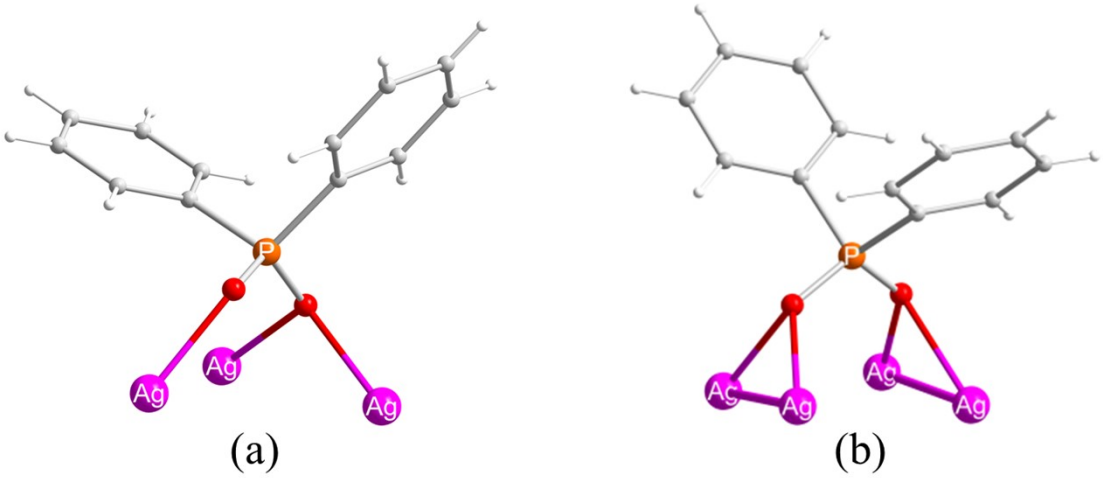

Figure S5. The μ_3:O_1,O_2 (a) and μ_4:O_2,O_2 (b) coordination modes of diphenylphosphonic acid ligands in cluster YL5.

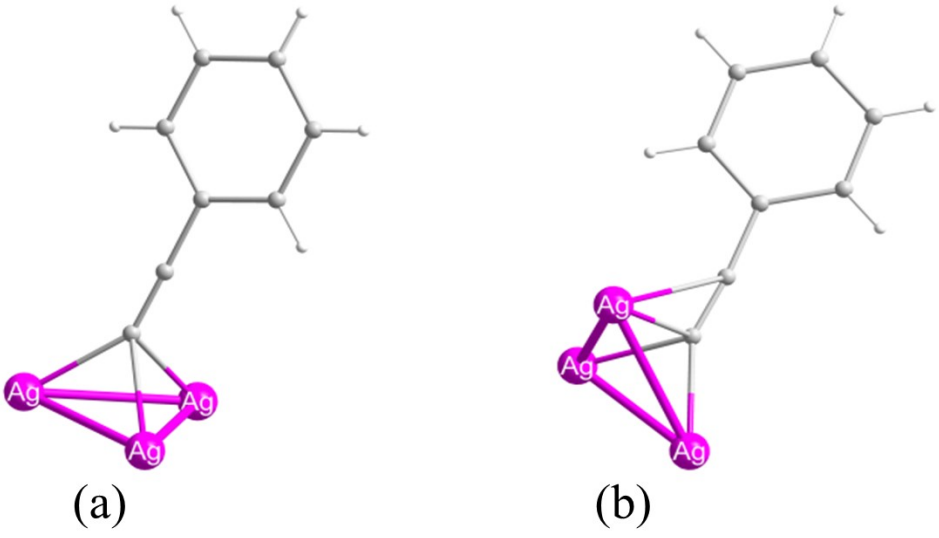

Figure S6. The μ_3-η^1,η^1,η^1 (a), and μ_3-η^1,η^1,η^2 (b) coordination modes of phenylethynyl ligands in cluster YL5.

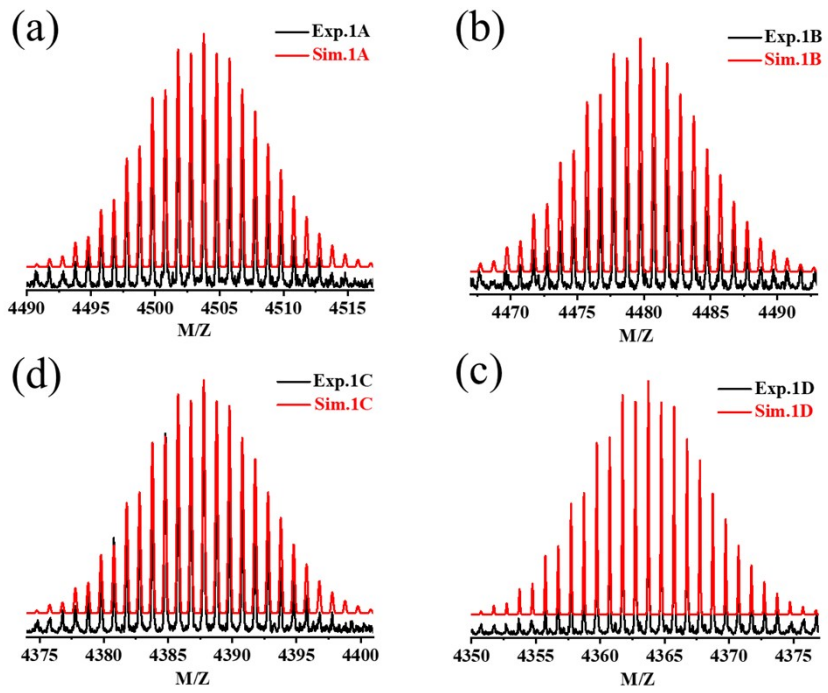

Figure S7. The full ESI-MS spectra with the experimental (blackline) and simulated (redline) isotopic patterns for species **1A-1D**. Note: **1M** = $(CrO_4)@Ag_{19}(PhC{\equiv}C)_7(Ph_2PO_2)_8(H_2O)(BF_4)_2(CH_3OH)$. (a-d) show four monovalent peaks:

1A = 4503.78: [**1M** – $2BF_4^-$ - $Ph_2PO_2^-$ - $PhC{\equiv}C^-$ - H_2O + $4CH_3OH$ + $3OH^-$]$^+$

1B = 4479.71: [**1M** – $2BF_4^-$ - $Ph_2PO_2^-$ - $PhC{\equiv}C^-$ - CH_3OH + H_2O + $2CH_3CN$ + $3OH^-$]$^{2+}$

1C = 4387.76: [**1M** – $2BF_4^-$ - $2PhC{\equiv}C^-$ + $4CH_3OH$ + $3OH^-$]$^+$

1D = 4363.72: [**1M** – $2BF_4^-$ - $2PhC{\equiv}C^-$ - CH_3OH + $2H_2O$ + $3OH^-$]$^+$

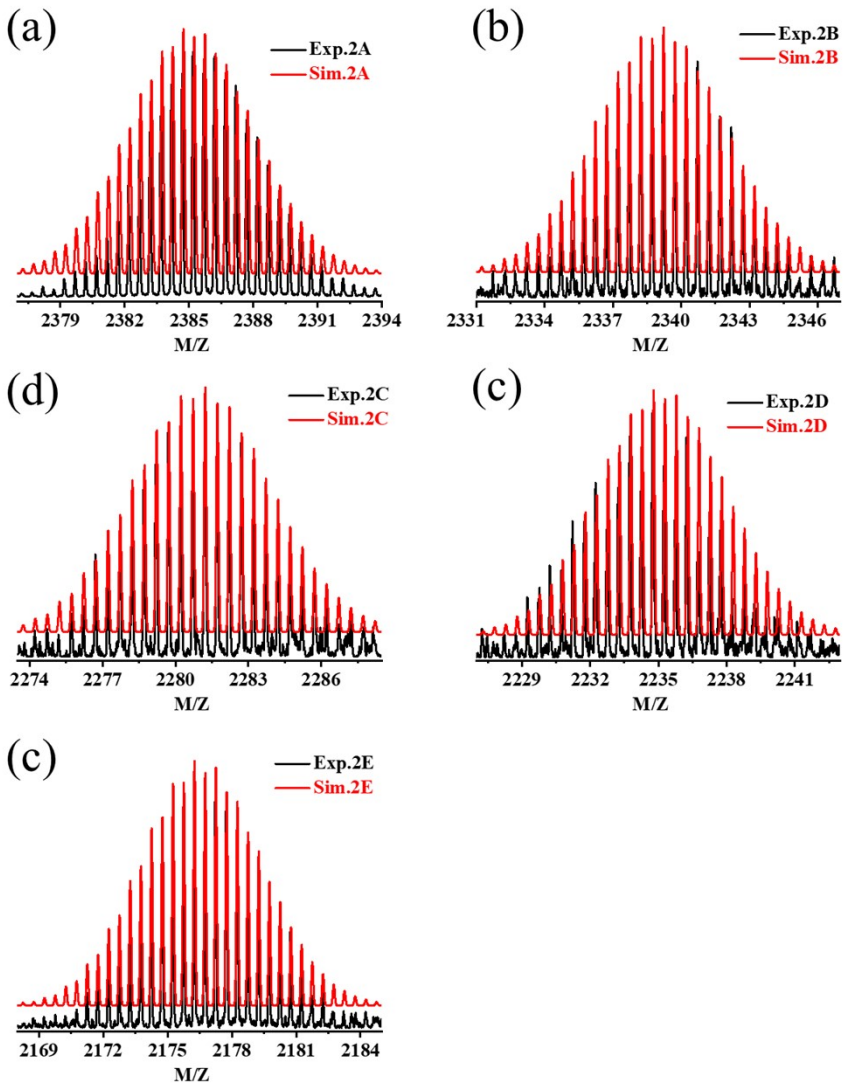

Figure S8. The full ESI-MS spectra with the experimental (blackline) and simulated (redline) isotopic patterns for species **2A-2E**. Note: **2M** = $(MoO_4)@Ag_{19}(PhC{\equiv}C)_9(Ph_2PO_2)_7(OTf)_2CH_3OH$. (a-e) show five monovalent peaks:

2A = 2385.19: [**2M** – OTf^- - $2Ph_2PO_2^-$ - $2CH_3OH$ + $3CH_3CN$ + $5CH_2Cl_2$ + OH^-]$^{2+}$

2B = 2339.21: [**2M** – OTf^- - $Ph_2PO_2^-$ - $PhC{\equiv}C^-$ - $2CH_3OH$ + $4CH_2Cl_2$ + OH^-]$^{2+}$

2C = 2281.20: [**2M** – OTf^- - $2Ph_2PO_2^-$ - $2CH_3OH$ + $4CH_2Cl_2$ + OH^-]$^{2+}$

2D = 2234.75: [**2M** - Ag^+ - OTf^- - $2Ph_2PO_2^-$ - CH_3OH + $4CH_2Cl_2$]$^{2+}$

2E = 2176.22: [**2M** - Ag^+ - $Ph_2PO_2^-$ - $PhC{\equiv}C^-$ - $2CH_3OH$ + $4CH_2Cl_2$ + OH^-]$^{2+}$

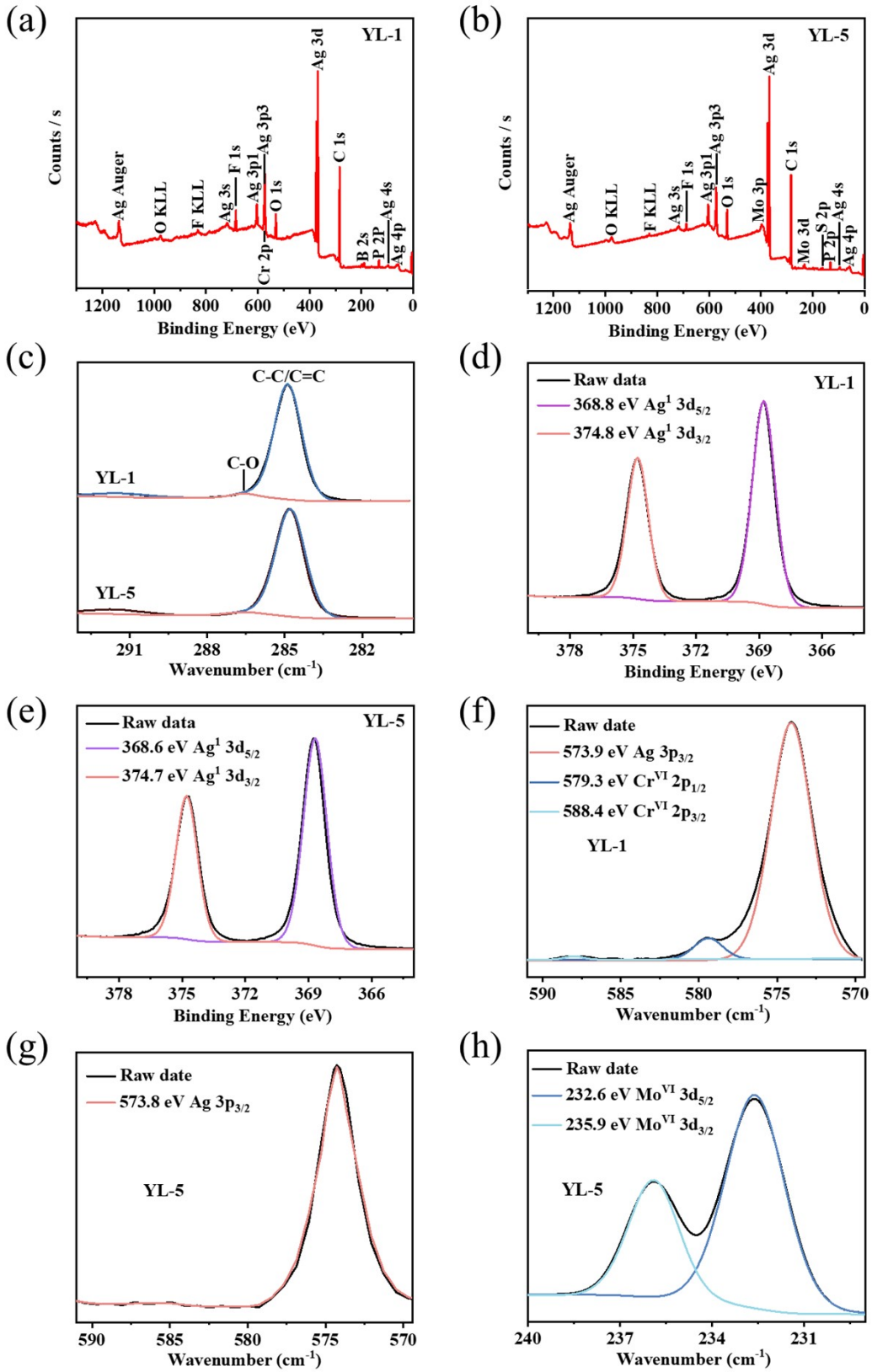

Figure S9. (a/b) XPS spectra of YL-1and YL-5 and detail enlargement of their (c) O 1s, (d/e) Ag3d, (f/g) Cr 2p, (h) Mo 3d.

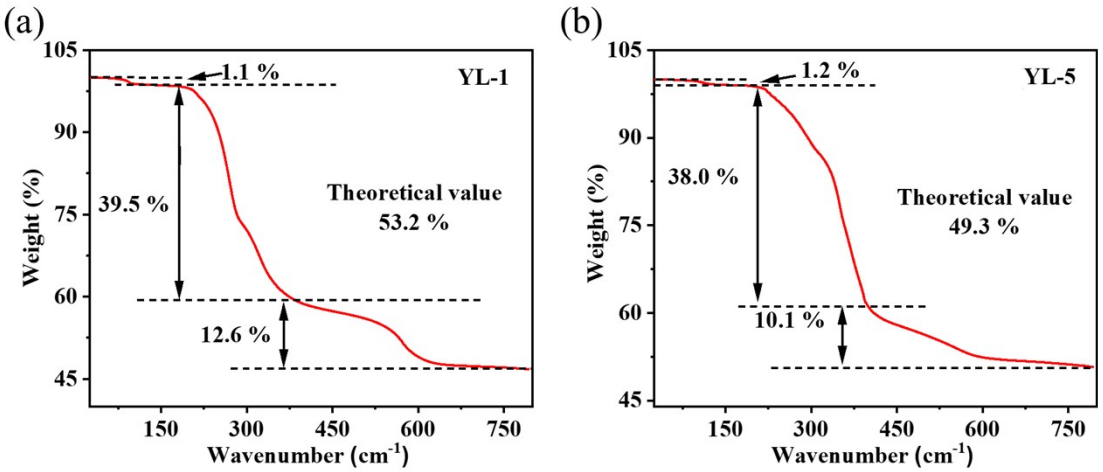

Figure S10. The TGA curves of YL-1 and YL-5.

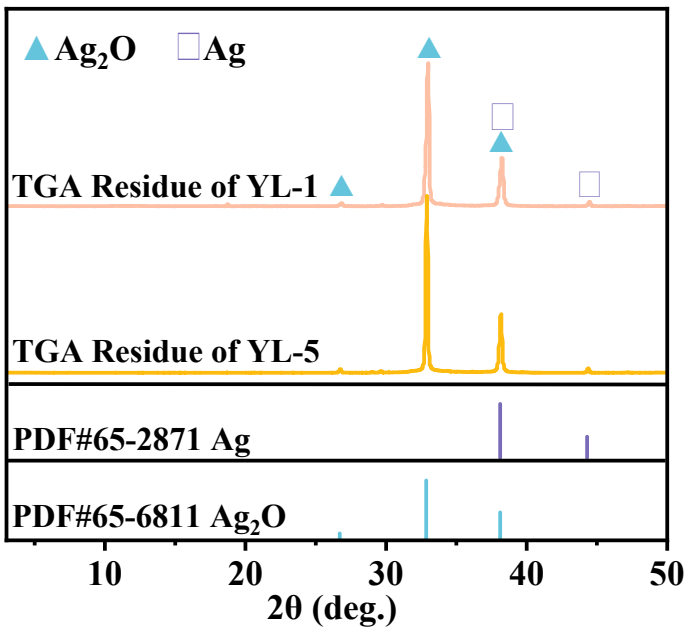

Figure S11. PXRD of TGA residue from YL-1 and YL-5.

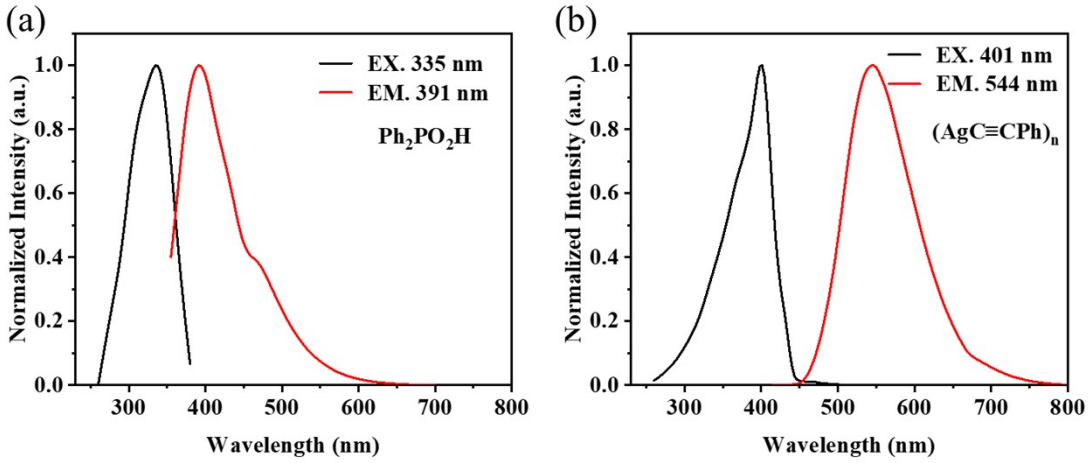

Figure S12. PL spectra of (a) Ph_2PO_2H and (b) $(AgC{\equiv}CPh)_n$ in the solid state at 77 K.

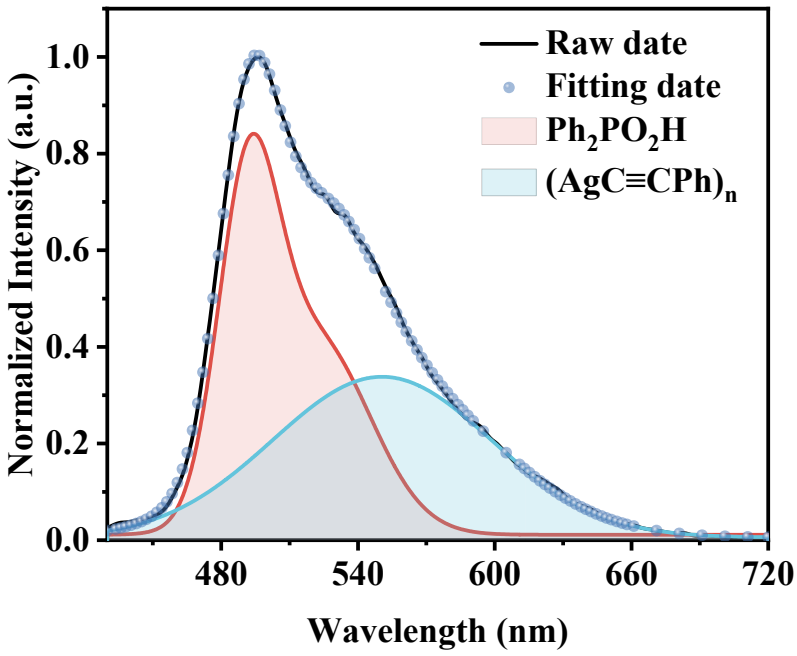

Figure S13. Luminescent Center Assignment Diagram for the Photoluminescent (PL) Spectrum of Solid-State cluster YL-5 at 77 K

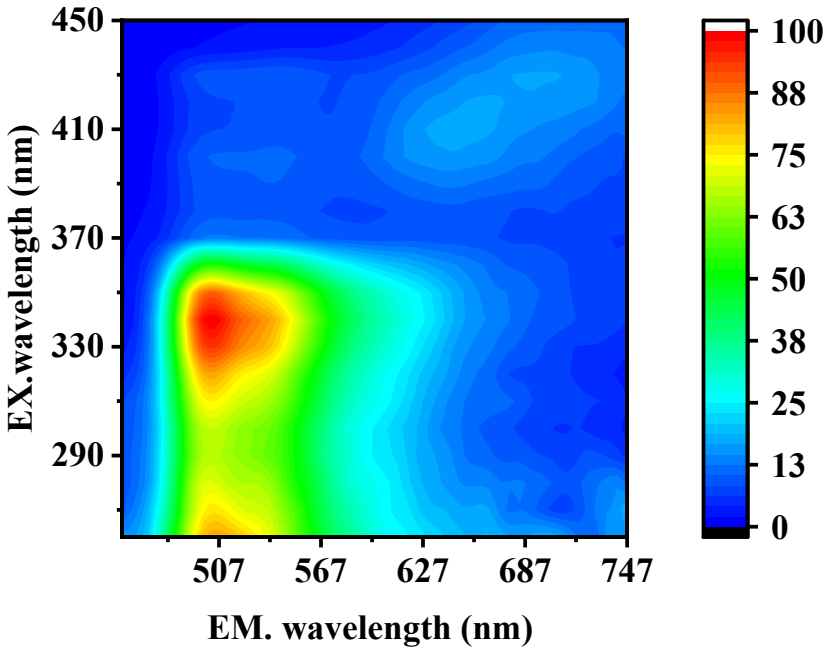

Figure S14. Temperature dependence of the emission wavelength of cluster YL-5.

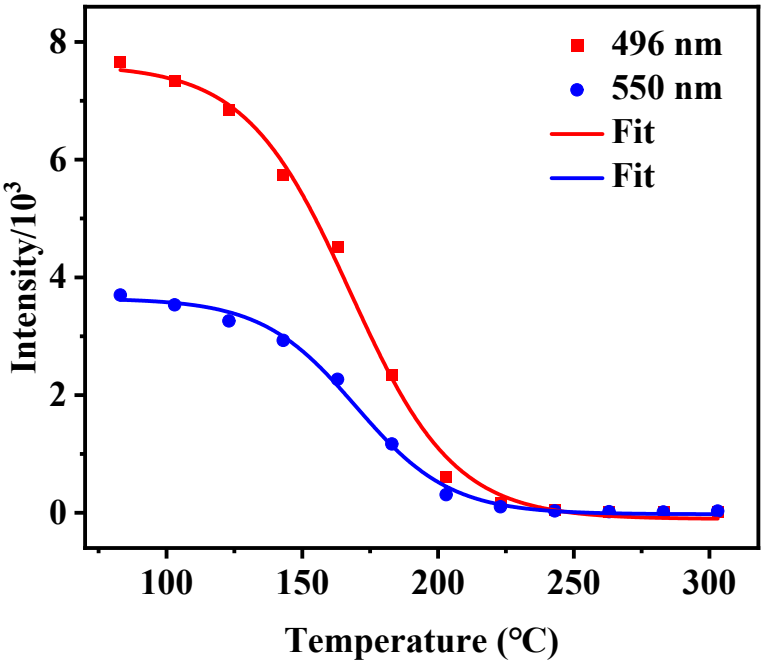

Figure S15. Temperature dependence of the emission intensity of cluster YL-5.

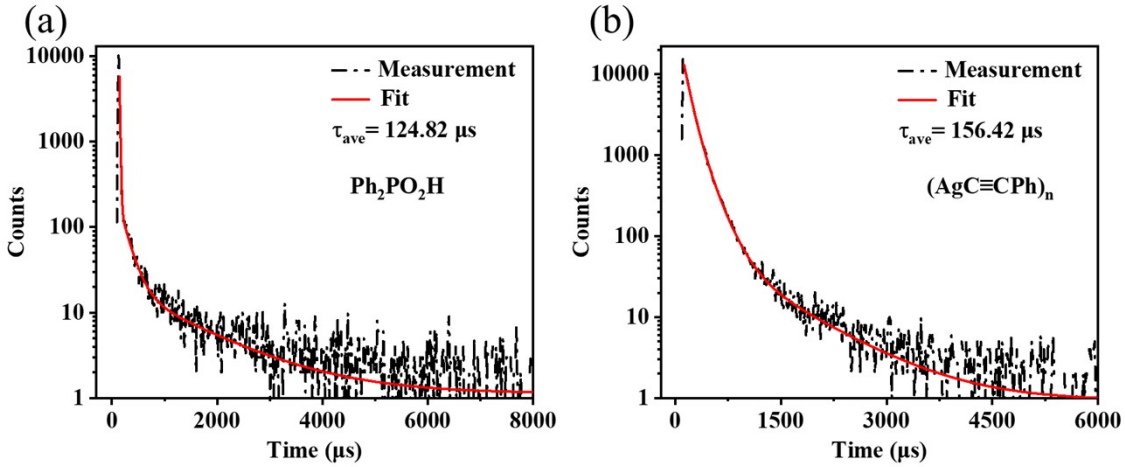

Figure S16. Luminescence decay curves of (a) Ph_2PO_2H and (b) $(AgC{\equiv}CPh)_n$ in the Solid State at 77 K

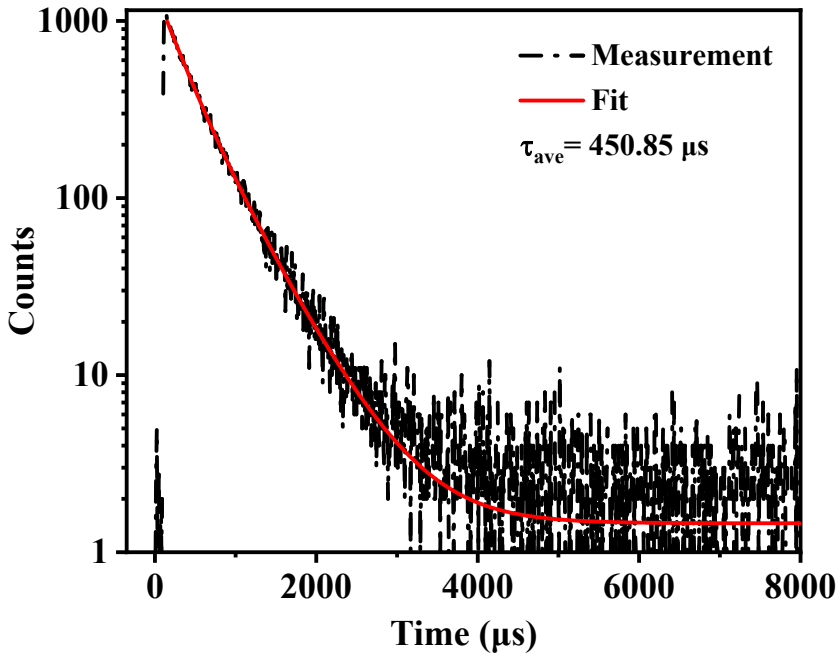

Figure S17. Luminescence decay curve of nanocluster YL-5 (Excitation: 346 nm) in the solid state at 77 K.

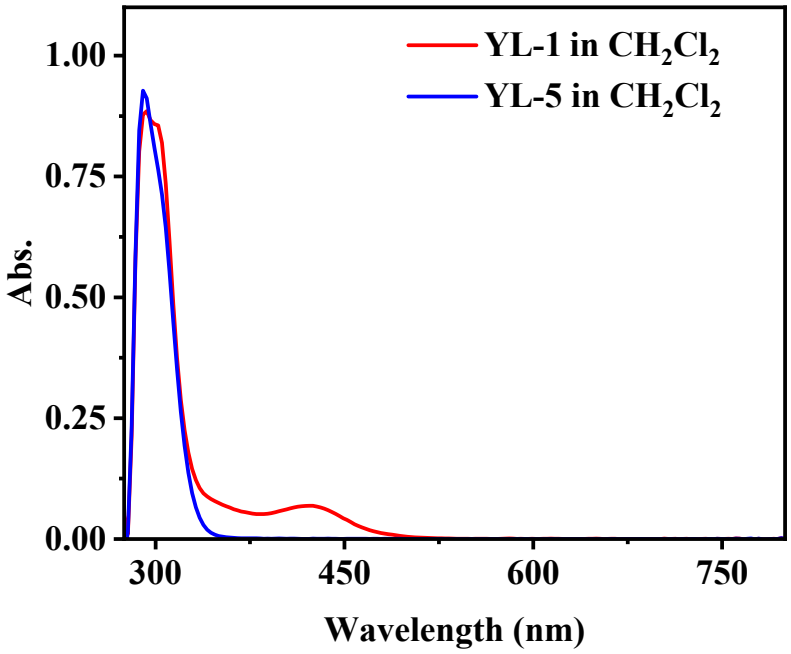

Figure S18. UV-Vis absorption spectra of YL-1 and YL-5 in dichloromethane solution

References

1. Xie, Y.-P.; Mak, T. C. W.. Synthetic and Structural Studies on High-Nuclearity Silver Ethynide Cluster Systems. *Journal of Cluster Science.* **2013**, *25*, 189-204.

2. Wang, Z.; Su, H.-F.; Tung, C.-H.; Sun, D.; Zheng, L.-S., Deciphering synergetic core-shell transformation from $[Mo_6O_{22}@Ag_{44}]$ to $[Mo_8O_{28}@Ag_{50}]$. *Nature Communications.* **2018**, *9*, 4407.

3. Wang Z., Alkan F., Aikens C. M., Kurmoo M., Zhang Z.-Y., Song K.-P., Tung C.-H., Sun D.. An Ultrastable 155-Nuclei Silver Nanocluster Protected by Thiacalix[4]arene and Cyclohexanethiol for Photothermal Conversion. *Angewandte Chemie International Edition*, **2022**, *61*, e202206742.

4. Wang Y.-X., Zhang J., Su H.-F., Cui X., Wei C.-Y., Li H., Zhang X.-M.. Photochemical Synthesis of Atomically Precise Ag Nanoclusters. *ACS Nano*. **2023**, *17*, 11607-11615.

5. Frisch, M.-J.; Trucks, G.-W.; Schlegel, H.-B.; Scuseria, G.-E.; Robb, M.-A.; Cheeseman, J.-R.; Scalmani, G.; Barone, V.; Petersson, G.-A.; Nakatsuji, H.; Li, X.; Caricato, M.; Marenich, A.-V.; Bloino, J.; Janesko, B.-G.; Gomperts, R.; Mennucci, B.; Hratchian, H.-P.; Ortiz, J.-V.; Izmaylov, A.-F.; Sonnenberg, J.-L.; Williams-Young, D.;

Ding, F.; Lipparini, F.; Egidi, F.; Goings, J.; Peng, B.; Petrone, A.; Henderson, T.; Ranasinghe, D.; Zakrzewski, V.-G.; Gao, J.; Rega, N.; Zheng, G.; Liang, W.; Hada, M.; Ehara, M.; Toyota, K.; Fukuda, R.; Hasegawa, J.; Ishida, M.; Nakajima, T.; Honda, Y.; Kitao, O.; Nakai, H.; Vreven, T.; Throssell, K.; Montgomery, J.-A.; Jr.; Peralta, J.-E.; Ogliaro, F.; Bearpark, M.-J.; Heyd, J.-J.; Brothers, E.-N.; Kudin, K.-N.; Staroverov, V.-N.; Keith, T.-A.; Kobayashi, R.; Normand, J.; Raghavachari, K.; Rendell, A.-P.; Burant, J.-C.; Iyengar, S.-S.; Tomasi, J.; Cossi, M.; Millam, J.-M.; Klene, M.; Adamo, C.; Cammi, R.; Ochterski, J.-W.; Martin, R.-L.; Morokuma, K.; Farkas, O.; Foresman, J.-B.; Fox, D.-J.. *Gaussian16*, Gaussian, Inc., Wallingford, CT, **2016**.

6. Becke, A.-D.. Density-Functional Exchange-Energy Approximation with Correct Asymptotic Behavior. *Physical Review A*. **1988**, *38*, 3098-3100.

7. Perdew, J.-P.. Density-functional approximation for the correlation energy of the inhomogeneous electron gas. *Physical Review B.* **1986**, *33*, 8822-8824.

8. Weigend, F.; Ahlrichs, R.. Balanced basis sets of split valence, triple zeta valence and quadruple zeta valence quality for H to Rn: Design and assessment of accuracy. *Physical Chemistry Chemical Physics*. **2005**, *7*, 3297-3305.

9. Grimme, S.. Semiempirical GGA-type density functional constructed with a long-range dispersion correction. *Journal of computational chemistry.* **2006**, *27*, 1787-1799.

10. Bloino, J.; Baiardi, A.; Biczysko, M.. Aiming at an accurate prediction of vibrational and electronic spectra for medium-to-large molecules: An overview. *International Journal of Quantum Chemistry*. **2016**, *116*, 1543-1574.

11. Adamo, C.; Barone, V.. Toward reliable density functional methods without adjustable parameters: The PBE0 model. *The Journal of chemical physics.* **1999**, *110*, 6158-6170.

12. Runge, E., Gross, E. K. U.. Density-Functional Theory for Time-Dependent Systems. *Physical Review Letters.* **1984**, *52*, 997.

13. Lu, T.; Chen F.-W.. Multiwfn: A multifunctional wavefunction analyzer. *Journal of Computation Chemistry.* **2012**, *33*, 580-592.

14. Yang, L.; Bigdeli F.; Yang X.-J.; Hou L.-L.; Ma Y.; Jiang W.-Y.; Li X.-H; Wang L.-X.; Yang T.; Wang K.-Z.; Wei J.-Y.; Morsali A.; Liu K.-G.. Molybdate-Templated Luminescent Silver Alkynyl Nanoclusters: Total Structure Determination and Optical Property Analysis. *Inorganic Chemistry*, **2024**, *63*, 7631-7639.

15. Jin J.-L.; Shen Y.-L.; Xie Y.-P.; Lu X.. Silver ethynide clusters constructed with fluorinated β-diketonate ligands. *CrystEngComm*, **2018**, *20*, 2036-2042.

16. Li X.-Y.; Wang Z.; Su H.-F.; Feng S.; Kurmoo M.; Tung C.-H.; Sun D.; Zheng N.-S.. Anion-templated nanosized silver clusters protected by mixed thiolate and diphosphine. *Nanoscale*, **2017**, *9*, 3601-3608.

17. Liao J.-H.; Chang H.-W.; You H.-C.; Fang C.-S.; Liu C. W.. Tetrahedral-shaped anions as a template in the synthesis of high-nuclearity silver (I) dithiophosphate clusters. *Inorganic Chemistry*, **2011**, *50*, 2070-2072.